Improved Perfusion-Weighted MRI by a Novel Double Inversion With Proximal Labeling of Both Tagged and Control Acquisitions

Geon-Ho Jahng, Xiao-Ping Zhu, Gerald B. Matson, Michael W. Weiner, and Norbert Schuff *

A novel pulsed arterial spin labeling (PASL) technique for multislice perfusion-weighted imaging is proposed that compensates for magnetization transfer (MT) effects without sacrificing tag efficiency, and balances transient magnetic field effects (eddy currents) induced by pulsed field gradients. Improved compensation for MT is demonstrated using a phantom. Improvement in perfusion measurement was compared to other PASL techniques by acquiring perfusion images from 13 healthy volunteers (nine women and four men; age range 29–64 years; mean age 45 ± 14 years) and second-order image texture analysis. The main improvements with the new method were significantly higher image contrast, higher mean signal intensity, and better signal uniformity across slices. In conclusion, this new PASL method should provide improved accuracy in measuring brain perfusion. Magn Reson Med 49:307–314, 2003.

Key words: PASL; double inversion; MT compensation; texture analyses; cerebral blood flow

Arterial spin labeling (ASL) MRI, both continuous (1) and pulsed (PASL), is a promising tool for quantitative measurements of brain perfusion in various neurodegenerative diseases, including Alzheimer's disease (2–4). Several PASL methods, including echo-planar imaging (EPI) and signal targeting with alternating RF (EPISTAR) (5,6), flow-sensitive alternating inversion recovery (FAIR) (7,8), and proximal inversion with a control for off-resonance effects (PICORE) (9), have been proposed for separating the signal of spin-labeled (tagged) blood from the signal of stationary tissue. In this work, EPISTAR, FAIR, and PICORE refer solely to a tag method rather than to a complete perfusion-weighted imaging (PWI) pulse sequence. A major problem with PASL, however, is that the RF pulses that tag arterial blood also induce modulations in the stationary brain tissue via magnetization transfer (MT), limiting accuracy in measuring perfusion (10). A common strategy to compensate for MT is to induce equal effects of MT in tag and control scans that ideally cancels out upon subtraction of the scans. EPISTAR and PICORE, depicted in Fig. 1, are two examples that apply this strategy. However, both methods have a weakness in compensating for MT. Although field gradients are matched between tagged and control scans in EPISTAR, a weakness is that the RF amplitudes differ by a factor of 2, thus causing potential differences in MT due to nonlinear spin responses (10). Similarly, although power and bandwidth are matched between tag and control scans in PICORE, eddy currents from unpaired slab-selective gradients can result in errors for MT compensation (11). Therefore, the first goal of this study was to design a new PASL method for multislice PWI with improved MT compensation.

Other problems with PASL that cause underestimation of perfusion are inflow of untagged blood into the image planes before mapping of the tagged blood is completed, and modulation of the perfusion signal due to variation in arterial transient time. The accuracy with which perfusion is measured can be improved by destroying blood transverse magnetization with periodic saturation pulses over a thin region proximal to the image planes, as proposed by Luh et al. (12) for QUIPSS II, termed Q2TIPS. Because periodic saturation and spin tagging are coupled, the second goal in this study was to compare our proposed PASL method with spin labeling by EPISTAR and PICORE in combination with a periodic saturation pulse.

Most previous experimental comparisons of perfusion methods were based on studies involving a few volunteers (9,13). Given the variation in brain perfusion among subjects, however, a relatively large number of studies are necessary to determine the significance of differences between methods. Furthermore, previous comparisons relied either on visual inspection of perfusion images (9,14) or on first-order image statistics, such as signal-to-noise ratio (SNR) measurements (13,15). However, visual comparisons are subjective, and comparisons based on SNR alone are limited in capturing the full complexity of image features that might change between different PASL methods. Therefore, the third goal was to determine whether the proposed PASL method provides significant improvements compared to PICORE and EPISTAR, given the biological variability of perfusion between subjects. This was accomplished by testing these PASL methods on a sufficiently large number of subjects, and by extending analysis of perfusion data to second-order texture statistics, including measurements such as contrast, entropy, correlation, and second angular moments (16).

PULSE SEQUENCE DESIGN

A diagram of the tag and control preparation with the proposed PASL method, termed double inversions with proximal labeling of both tag and control images (DIPLOMA) is

MR Unit, VA Medical Center, University of California–San Francisco, San Francisco, California.

Grant sponsor: NIH; Grant numbers: AG10897; AG12435.

*Correspondence to: Norbert Schuff, Ph.D., MR Unit, VA Medical Center, 114M, University of California–San Francisco, 4150 Clement St., San Francisco, CA 94121. E-mail: nschuff@itsa.ucsf.edu

Received 18 April 2002; revised 4 September 2002; accepted 8 September 2002.

DOI 10.1002/mrm.10339
Published online in Wiley InterScience (www.interscience.wiley.com).

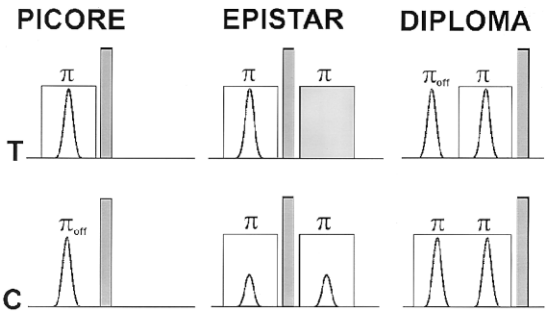

FIG. 1. PASL with PICORE, EPISTAR, and DIPLOMA. Shown are B_1- amplitudes of tag (T) and control (C) RF pulses for spin inversion. Off-resonance inversion is indicated by π_{off}. Slab-selective gradients are indicated by transparent squares, while spoiler gradients are shown in gray. In EPISTAR, RF pulse amplitudes for control and tag differ by a factor of 2.

shown in Fig. 1. Figure 1 also shows tag and control preparations of PICORE and EPISTAR. In detail, the tag scan of DIPLOMA includes 1) a spectral-selective inversion pulse off-resonance to water (π_{off} in Fig. 1), inducing an MT effect and no inverse magnetization of blood water; and 2) a slab-selective inversion pulse on-resonance (π in Fig. 1) with the same amplitude as π_{off}, again inducing an MT effect, but with inverse magnetization (tag) of blood water. In contrast, the control scan of DIPLOMA consists of two slab-selective inversion pulses on-resonance, both of which induce MT effects but no net magnetization change of blood water. With the condition that the difference between off- and on-resonance frequency is small compared to the frequency distribution of MT, tag and control scans generate nearly equal amounts of MT that cancel upon subtraction of the tag and control images. Furthermore, because pulsed gradients were applied in both the tag and control scans, the effects of eddy currents cancel to a large extent as well. Finally, because all four RF inversion pulses are of the same power, the slice profiles in the tag and control scans are virtually identical.

The whole sequence for PWI, including PASL and the imaging part of Q2TIPS (12), is depicted in Fig. 2a. First, two saturation pulses (SAT1) destroy magnetization in the image planes to reduce background noise. Thereafter, PASL is applied for tag blood within a region proximal to the image planes. Following PASL and a inversion time (TI) TI1, 14 periodic saturation pulses (SAT2) are applied across a 20-mm band at the distal edge of the tag region to destroy magnetization of untagged blood that flows out of the tag region, as proposed by Luh et al. (12), and to clearly define the length of the tag region. After another delay time (TD), TD1, a standard EPI scheme is used to acquire multislice PW images. Before the sequence is repeated for signal averaging, two RF pulses are applied to saturate the image planes (SAT1), followed after another delay, TD2, with gradient pulses to destroy residual transverse magnetization (17). An example of tag and image slice positions for measuring perfusion in the cerebrum are sketched in Fig. 2b. PASL was accomplished for all three methods using adiabatic hyperbolic secant pulses that were generated with software described in Ref. 18 using the following parameters: side-to-width parameter (μ) = 10, pulse bandwidth factor (β) = 630 s^{-1}, and pulse duration = 12.8 ms, requiring an RF field strength (B_1) of approximately 14 μT that resulted in combination with a magnetic field gradient (G_1) of 0.41 mT/m in a 90-mm-wide tag region.

METHODS

Experiments on phantoms and volunteers were performed on a standard 1.5T MR system (Siemens Vision, Erlangen, Germany) using a circularly polarized head coil for RF transmission and reception. The Committee for Human Research of the University of California approved the study, and all volunteers provided written informed consent before participating in this study.

Phantom Studies

Compensation for MT

A 3% agarose phantom with tap water doped by 0.45 mM/L of copper sulfate to maintain T_1 = 1056.0 ± 5.5 ms (19) was used to compare the abilities of DIPLOMA, PICORE, and EPISTAR for canceling out MT effects for

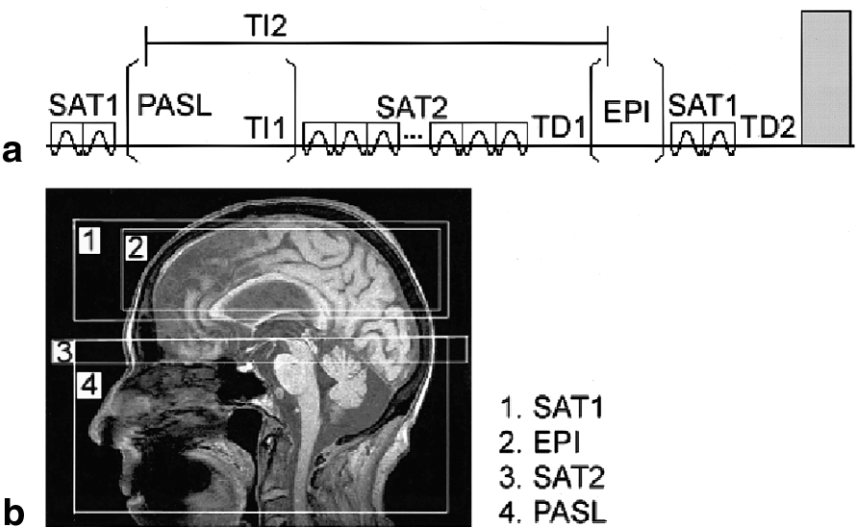

FIG. 2. (**a**) Perfusion imaging sequence and (**b**) arrangement for perfusion imaging. Indicated are spin saturation (SAT1 and SAT2), PASL, and EPI acquisition periods. TI1 and TI2 are spin inversion times, and TD1 and TD2 are delay times that determine overall TR. Transparent squares indicate slab-selective gradients, and the gray area indicates a spoiler gradient.

single-slice acquisition. First, the MT spectrum of the phantom was determined over a frequency range of zero Hz to 20 kHz by varying within this range the frequency of a hyperbolic secant inversion pulse (20.48 ms long, corresponding to 0.85 kHz bandwidth) applied in the absence of a gradient and imaging signal intensity (SI) using a 3D fast low-angle shot (FLASH) sequence (TR = 150 ms, TE = 6 ms, and excitation = 45°) (20). MT magnitudes were expressed relative to the unperturbed signal S_{off} of the phantom according to MT = $100*(S_{off} - S_{on})/S_{off}$, with S_{on} representing the perturbed signal after an inversion pulse was applied. Second, the following studies were repeated for each sequence: 1) a reference image without tag and control pulses was acquired (reference mode); 2) an image uncompensated for MT was acquired, using a 550 Hz off-resonance tag pulse but no control pulse (MT mode); and 3) an image compensated for MT was acquired, using tag and control pulses in regular mode (compensation mode). Except for the three different PASL schemes, the remainder of the pulse sequence was fixed with respect to timing and EPI acquisition. Saturation pulses were turned off for each PASL scheme. A single image slice was acquired with TI1 = 0.685 s, TI2 = 1.2 s, a 50-mm-wide tag region, and 20 mm distal from the image slice. Differences between the sequences in MT and compensation mode were expressed relative to the mean image intensity in reference mode (S_{ref}) and transformed into a *Z*-score, according to $(S_{max} - S_{ref})/STD_{ref}$ for the MT mode and $(S_{pwi} - S_{ref})/STD_{ref}$ for the compensation mode, where STD_{ref} is the standard deviation (SD) of the image intensity in reference mode. A *Z*-score of zero indicates perfect MT compensation, and a *Z*-score of 1 implies 1 SD from perfect MT compensation.

Interaction Between Periodic Saturation and PASL

To test interactions between periodic saturation pulses and the different PASL schemes, experiments were performed on a doped-water phantom (T_1 = 1068.9 ± 4.3 ms) and the agarose phantom with an increasing number of periodic saturation pulses from 10 to 20 in steps of 2. Imaging parameters in these experiments were: TR = 2.5 s, TE = 15 ms, TI1 = 780 ms, TI2 = 1500 ms, acquisition of five slices, each 5 mm thick with a 5-mm gap between slices, and 34 acquisitions. The gap between the imaging plane and the tag plane was 20 mm. SI variations in subtraction images were observed with varying the saturation pulses.

Human Studies

Interaction Between Periodic Saturation and PASL

Interaction between the periodic saturation pulses and the different PASL methods were tested on a volunteer, using the same acquisition parameters as in the phantom studies. The extent to which intensity of perfusion varied as a function of the number of periodic saturation pulses for each PASL method was determined by computing a coefficient of variation (COV) (SD divided by mean intensity) of perfusion SI for each image slice.

Comparison Between the PASL Methods

In order to compare the ability of the different PASL methods to measure perfusion, 13 healthy volunteers (nine women and four men; age range 29–64 years; mean age 45 ± 14 years) were studied using the three PASL schemes, while the rest of the PWI sequence parameters were kept identical. Following an initial scout scan for anatomical orientation, PWI acquisitions with PICORE, EPISTAR, and DIPLOMA were performed in rapid succession in a single session. Volunteers were asked to close their eyes and relax during scans to achieve similar conditions between scans of resting-state blood flow. The PWI acquisition parameters were: TR = 2.5 s, TE = 15 ms, TI1 = 780 ms, TI2 = 1500 ms, and 14 periodic saturation pulses; tag was accomplished over a 90-mm-wide region using hyperbolic secant pulses with the parameters described previously. At a 15-mm distance from the tag region, PWI of five axially-oblique slices (each 8 mm thick, 2 mm apart, and oriented 10° off the anterior-posterior commissure line) were acquired with a resolution of 4.6 × 2.3 mm^2 over a field of view (FOV) of 225 × 300 mm^2. Following acquisition and image reconstruction, the data were transferred to an off-line workstation for image analysis.

Statistical Analysis

PW images of the volunteers were evaluated using texture analysis (16,21,22). The the first-order textures included mean SI (MSI) and COV of SI (COVSI). The second-order textures included contrast, correlation, entropy, and angular second moment (ASM). Definitions of the different textures were programmed in IDL5.2 (Research Systems, Inc., Boulder, CO) and are summarized in the appendix. In addition, second-order texture values at 0°, 45°, 90°, and 135° angular directions were averaged for each slice and subject. Differences between the PASL methods were tested using paired *t*-tests. Furthermore, to determine whether the difference between methods remained significant in the presence of variability between subjects, we performed two-factor analysis of variance (ANOVA) tests (method and subjects), followed by post-hoc pairwise comparisons of the methods. The level of significance was raised to $P = 0.05/6 \leq 0.008$ to reduce the risk for significant findings by chance (Bonferoni correction).

RESULTS

Phantom Studies

The spectral distribution of MT between 50 Hz and 1.3 kHz in the agarose phantom is shown in Fig. 3. This shows that at 550 Hz, which was used as the offset frequency for the tag pulse, the MT magnitude was about 39% of maximum. Table 1 lists the results from uncompensated (MT mode) and compensated MT measurements for each PASL scheme. This demonstrates that the best MT compensation was achieved with DIPLOMA, as indicated by the smallest *Z*-score, although absolute intensity from uncompensated MT was highest for DIPLOMA. The number of periodic saturation pulses did not affect SI in any PASL method.

Human Studies

Interaction Between Periodic Saturation and PASL

The graphs in Fig. 4 show the effect of increasing the number of periodic saturation pulses on SI in PW images for DIPLOMA (Fig. 4a), EPISTAR (b), and PICORE (c), and

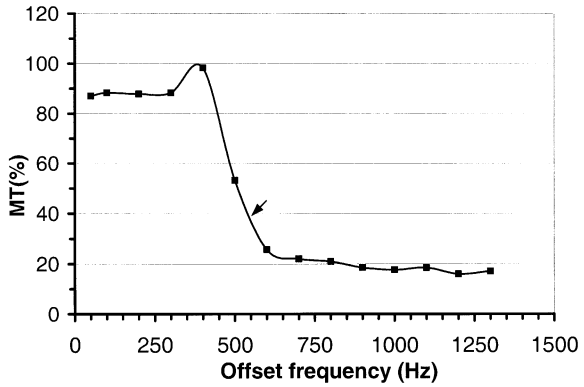

FIG. 3. Spectral distribution of MT effects in the agarose phantom. MT compensation of the different PASL methods was tested with 550 Hz frequency offset for tag pulses (arrow, corresponding to a roughly 39% MT effect).

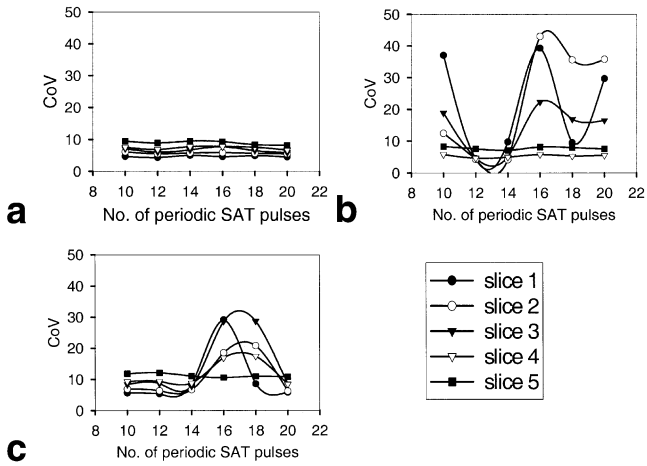

FIG. 4. Variation of perfusion signal intensities as a function of number of periodic saturation pulses in multislice PWI with different PASL methods: (**a**) DIPLOMA, (**b**) EPISTAR, and (**c**) PICORE. Data are from a young volunteer. Variation of the perfusion signal in each slice is expressed as a COV. Slice 5 is most proximal to the tag region.

indicate large differences between the PASL methods. The smallest signal variability was achieved with DIPLOMA, indicating minimal interaction between period saturation and PASL, and thus consistency in measuring perfusion.

Comparison Between the PASL Methods

Representative PWI data from a volunteer (a 28-year-old female) obtained with PASL by DIPLOMA, EPISTAR, and PICORE are shown in Fig. 5a–c, respectively. Images were scaled to the same brightness for better comparison. This shows a higher perfusion contrast in regions of gray and white matter with DIPLOMA than with other PASL methods. Furthermore, overall image intensity across slices varied less with DIPLOMA than with other PASL methods. This is also seen in Table 2, which lists mean intensity values of PWI data for each slice from 13 subjects, together with the COVs (SD divided by the mean intensity from five slices) for each PASL method, indicating the extent of intensity variability from slice to slice.

The results from a texture analysis of the PWI data from the volunteers are listed in Table 3 for each PASL method. MSI was 8% higher with DIPLOMA ($P = 0.003$, by paired t-test) than with EPISTAR, indicating improved sensitivity in measuring perfusion. The difference in MSI between DIPLOMA and EPISTAR remained significant when variability between the subjects was considered ($F[1,12] = 13.6$, $P < 0.003$). DIPLOMA and PICORE had comparable MSI values ($P = 0.05$). COVSI was 28% lower with DIPLOMA ($P < 0.001$) than with PICORE, indicating less image noise. This difference between DIPLOMA and PICORE remained also significant when subject variability was considered. ($F[1,12] = 70.0$, $P < 0.001$). Compared to EPISTAR, however, DIPLOMA had an approximately 21% higher COVSI value ($P < 0.001$). Of the second-order textures, contrast was 23% higher with DIPLOMA ($P < 0.008$) than with EPISTAR, indicating better image quality. This difference between DIPLOMA and EPISTAR remained significant when subject variability was considered ($F[1,12] = 10.0$, $P \leq 0.008$). In contrast, DIPLOMA and PICORE had comparable contrast values ($P = 0.8$). Entropy was 1.7% higher with DIPLOMA than with PICORE ($P < 0.001$), indicating increased image complexity. This difference remained also significant when subject variability was considered ($F[1,12] = 19.7$, $P < 0.001$). In contrast, DIPLOMA and EPISTAR had comparable values for entropy ($P = 0.1$). Correlation yielded no significant difference between the methods. Finally, angular second moment (ASM) was about 15% lower with DIPLOMA than with PICORE ($P = 0.006$), indicating improved image uniformity. This difference between DIPLOMA and PICORE also remained significant when subject variability was considered ($F[1,12] = 11.0$, $P < 0.006$). In contrast, DIPLOMA and EPISTAR had comparable ASM values ($P = 0.5$). In summary, several image textures indicated better or similar image quality with DIPLOMA as compared to PICORE or EPISTAR. However, COVSI was best with EPISTAR.

Table 1
Magnetization Transfer (MT) Effects for Different PASL Schemes Measured on an Agarose Phantom

PASL	Tagging frequency offset	MT mode[a]	Compensation mode[b]
DIPLOMA	550 Hz	28.4	1.1
EPISTAR	550 Hz	15.7	6.1
PICORE	550 Hz	16.4	3.8

[a]MT mode (S_1): MT measurements with tag pulse *on* and control pulse *off*.
[b]Compensation mode (S_2): MT measurements with tag and control pulses *both on;* Values are in Z-scores:= $(S_{1\ or\ 2} - S_{ref})/STD_{ref}$,; STD_{ref} is the standard deviation of intensities in the reference image mode (S_{ref}) with tag and control pulses *both off.*

DISCUSSION AND CONCLUSIONS

The main findings of this study were that DIPLOMA improved MT compensation, as shown with phantoms, and improved the quality of PWI, as demonstrated with image texture analysis of MRI data from volunteers.

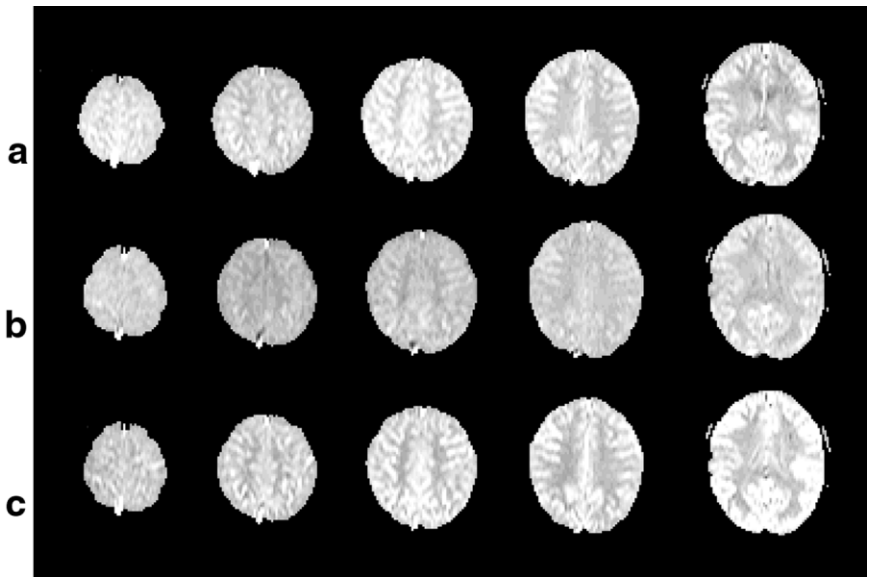

FIG. 5. Representative PW images obtained with (**a**) DIPLOMA, (**b**) EPISTAR, and (**c**) PICORE from a volunteer (28-year-old female). Images are scaled to the same brightness for better comparison, showing superior contrast and uniformity across slices with DIPLOMA.

Two major problems with PASL are a weakness in compensating for MT effects, and poor balance of eddy currents between tag and control scans. Both problems are amplified with PICORE. With EPISTAR, eddy currents are fully removed, but MT effects may remain because of nonlinear spin response due to different pulse amplitudes in tag and control scans. As regards the handling of eddy currents, DIPLOMA is better than PICORE but not as effective as EPISTAR. In contrast to PICORE, pulse gradients are applied in both tag and control scans in DIPLOMA, partially balancing the eddy currents. However, eddy current compensation is better with DIPLOMA than with EPISTAR because different pulses are used on the slice gradient channel. For MT compensation, DIPLOMA has the advantage over EPISTAR in not relying on MT response linearity to irradiation. However, MT compensation with DIPLOMA is not perfect, because half of the RF irradiation in the tag scan is applied without slab selection; therefore, different imaging slices may depict the irradiation at different frequency offsets. This is fully compensated for by EPISTAR. Whether MT compensation is better with DIPLOMA or EPISTAR depends on the relative contributions from nonlinear spin response and frequency offsets to MT. Compared to PICORE, MT compensation is better with DIPLOMA, because the other half of the RF irradiation in the tag scan is applied with slab selection, and therefore partial compensation of frequency offsets between imaging slices is achieved.

Another approach for MT compensation is the transfer insensitive labeling technique (TILT), which uses two gradient pulses of opposite polarity in combination with two slice-selective 90° excitation pulses of opposite phase in both tag and control scans (23). However, simulations have shown that MT compensation is limited with TILT, as RF frequency offset for slice selection increases (24). In addition, TILT may compromise tagging efficiency, because 90° excitation pulses are more susceptible to B_1 inhomogeneity than are adiabatic inversion pulses.

Although it is difficult to quantify MT compensation in perfusion studies on humans, the results from texture analysis suggest that DIPLOMA is similar to or better than other techniques in compensating for differences between tag and control scans, including MT effects. Especially notable was an improvement in image contrast with DIPLOMA as compared to EPISTAR. A possible limitation of DIPLOMA is decreased efficiency of blood tagging, because the extended duration with two inversion pulses increases T_1 relaxation during tag. However, higher RF pulse power in combination with stronger gradients can be used to shorten duration (25–27).

Previously, Luh et al. (12) used periodic saturation pulses over a narrow region at the distal edge of the tag region that increased the precision in measuring perfu-

Table 2
Slice Uniformity of Perfusion Images by Different PASL Methods

PASL	Slices					CoV (%)
	1	2	3	4	5	
DIPLOMA	1.00 ± 0.06	0.98 ± 0.06	1.00 ± 0.06	0.99 ± 0.05	0.99 ± 0.04	1.04
EPISTAR	0.93 ± 0.04	0.88 ± 0.06	0.91 ± 0.05	0.93 ± 0.04	0.98 ± 0.06	3.74
PICORE	1.00 ± 0.08	0.97 ± 0.08	0.99 ± 0.08	1.01 ± 0.08	1.13 ± 0.09	5.85

Perfusion signal intensities (means ± SD) averaged from 13 subjects and normalized to the first slice intensity in DIPLOMA. Variation from slice to slice is expressed as a coefficient of variation (CoV = SD divided by the mean intensity from five slices).

Table 3
Comparison of Perfusion Weighted Images Obtained With Different PASL Methods on 13 Volunteers Using First and Second Orders of Texture Analysis*

Feature	DIPLOMA	EPISTAR	PICORE	Δ(D-E)	Δ(D-P)
MSI	1.00 ± 0.05	0.92 ± 0.06	1.01 ± 0.08	8[b]	1
COVSI	0.14 ± 0.03	0.11 ± 0.03	0.18 ± 0.05	21.4[b]	−28.6[a]
Contrast	187 ± 126	144 ± 81	186 ± 129	23[b]	0.5
Entropy	2.88 ± 0.15	2.86 ± 0.13	2.83 ± 0.15	0.7	1.7[a]
Correlation	0.63 ± 0.06	0.65 ± 0.07	0.64 ± 0.07	−3.2	−1.6
ASM	1.81 ± 0.87	1.86 ± 0.72	2.08 ± 0.95	−2.8	−14.9[a]

*Data are means and SDs of 13 subjects and five slices per subject. Values of second order textures (Contrast, Entropy, Correlation, ASM) are the average from four directions in the image plane (0°, 45°, 90°, 135°).
[a]$P \leq 0.008$ DIPLOMA vs. PICORE;
[b]$P \leq 0.008$ DIPLOMA vs. EPISTAR
MSI, mean signal intensities, normalized to MSI of DIPLOMA; COVSI, coefficient of variation of signal intensity; ASM = angular second moment; Δ(D-E), difference in image textures between DIPLOMA and EPISTAR in percent relative to DIPLOMA; Δ(D-P), difference in image textures between DIPLOMA and PICORE in percent relative to DIPLOMA.

sion. This was attributed in part to a reduction of untagged blood flowing into the image plan, diluting the perfusion signal from tagged blood. As data from a volunteer show (Fig. 4), care must be taken when combining periodic saturation pulses with different PASL methods. Results showed that DIPLOMA is relatively insensitive to an interaction with periodic saturation pulses, while PICORE and EPISTAR exhibited higher sensitivity. This effect is probably a combination of inversion pulse, T_1 relaxation, and arterial blood velocity, although the details remain unclear. Further investigations are necessary to better elucidate this aspect. The number of periodic saturation pulses also appears to be important. If this number is too small, the time for saturation is too short and untagged and unsaturated blood may reach the imaging sections, diluting the perfusion signal. In contrast, if the number of pulses is too large, the time for saturation may become too long, and the perfusion signal decreases due to T_1 relaxation (12).

While comparisons of perfusion methods have been performed before (13,15,28,29), differences between the methods have not been related to perfusion variability between subjects. However, without considering subject-to-subject variability the advantage of a method for measuring perfusion differences between groups is difficult to establish. The current study related differences between the methods to differences in a reasonably large number of subjects. Furthermore, first- and second-order image texture analysis expressed differences between PWI data quantitatively for a range of different image features. The most significant improvement of DIPLOMA was increased perfusion contrast between gray and white matter. A high gray/white matter contrast in PW images is particularly important for studies of brain diseases that are expected to present changes in cerebral blood flow—specifically in cortical gray matter, such as in Alzheimer's disease, or in white matter, such as in ischemic vascular dementia.

Another significant improvement of DIPLOMA was increased MSI and increased signal uniformity across slices. Both improvements are important for measuring regional variations in perfusion accurately. This is useful in, for example, Alzheimer's disease, which often shows reduced blood flow in temporo-parietal lobe regions while frontal and occipital lobes are spared (30). Other improvements of DIPLOMA were increased entropy and decreased ASM as compared to PICORE. Increased entropy implies that information content in the image has increased. Decreased ASM indicates that the dynamic range of image intensities has increased. Improvements of both entropy and ASM suggest that the ability of measuring regional perfusion differences in the volunteers was better with DIPLOMA than with the other methods.

In conclusion, this new PASL method showed improved compensation for MT effects, and improvements in some imaging features (especially higher perfusion contrast) compared to other methods. Therefore, accuracy in measurement of cerebral blood flow should increase with the new method.

ACKNOWLEDGMENTS

We thank Drs. Dieter J. Meyerhoff and Govindaraju Varanavasi for their help in designing the phantoms.

APPENDIX

First-Order Image Textures Used in This Study

1. MSI (22)

$$MSI = \frac{1}{N} \sum_{i=0}^{N_i-1} \sum_{j=0}^{N_j-1} p(i, j)$$

where $p(i,j)$ is the gray level in image pixel (i,j), N_i and N_j are the number of pixels for i and j, respectively, and $N = N_i * N_j$ is the total number of image pixels.

2. COVSI

$$COVSI = \frac{STD}{MSI}$$

where STD is the SD of SI in the image.

$$STD = \sqrt{\frac{\sum_{i=0}^{N_i-1}\sum_{j=0}^{N_j-1}(p(i,j) - MSI)^2}{N-1}}$$

This represents a COVSI in the image.

Second-Order Textures Used in This Study

Second-order texture can be derived from a co-occurrence matrix $C(i,j)$, which reflects the frequency in which gray level combinations occur in pairs of pixels, separated by a given distance between pixels. $C(i,j)$ is calculated for 0°, 45°, 90°, and 135° directions in the image plane, yielding four matrixes. In this study, the distance was fixed to one pixel, and textures derived from $C(i,j)$ of the four directions were averaged.

1. Contrast (22)

$$CONTRAST = \sum_{i=0}^{N_i-1}\sum_{j=0}^{N_j-1}\{(i-j)^2 C(i,j)\}$$

This represents the contrast in an image. Contrast increases with larger gray level differences in an image.

2. Correlation (21)

$$CORRELATION = \frac{\sum_{i=0}^{N_i-1}\sum_{j=0}^{N_j-1}(i-\mu_i)(j-\mu_j)C(i,j)}{\sigma_i\sigma_j}$$

$$\mu_i = \sum_{i=0}^{N_i-1}\left\{ i\left[\sum_{j=0}^{N_j-1} C(i,j)\right]\right\}$$

$$\mu_j = \sum_{j=0}^{N_j-1}\left\{ j\left[\sum_{i=0}^{N_i-1} C(i,j)\right]\right\}$$

$$\sigma_i^2 = \sum_{i=0}^{N_i-1}\left\{ (i-\mu_i)^2\left[\sum_{j=0}^{N_j-1} C(i,j)\right]\right\}$$

$$\sigma_j^2 = \sum_{j=0}^{N_j-1}\left\{ (j-\mu_j)^2\left[\sum_{i=0}^{N_i-1} C(i,j)\right]\right\}$$

This represents a measure of the relationship between pixel gray levels. Correlation increases with increasing image heterogeneity.

3. Entropy (16)

$$ENTROPY = -\sum_{i=0}^{N_i-1}\sum_{j=0}^{N_j-1}\{C(i,j)\log(C(i,j))\}$$

This represents a measure of homogeneity among pixel gray levels. Entropy increases with increasing image complexity.

4. ASM (16)

$$ASM = \sum_{i=0}^{N_i-1}\sum_{j=0}^{N_j-1}\{C(i,j)\}^2$$

This represents a measure of clustering of pixel gray levels. ASM increases with a decreasing dynamic range of pixel gray levels.

REFERENCES

1. Williams DS, Detre JA, Leigh JS, Koretsky AP. Magnetic resonance imaging of perfusion using spin inversion of arterial water. Proc Natl Acad Sci USA 1992;89:212–216.
2. Sandson TA, O'Connor M, Sperling RA, Edelman RR, Warach S. Noninvasive perfusion MRI in Alzheimer's disease: a preliminary report. Neurology 1996;47:1339–1342.
3. Detre JA, Alsop DC, Vives LR, Maccotta L, Teener JW, Raps EC. Noninvasive MRI evaluation of cerebral blood flow in cerebrovascular disease. Neurology 1998;50:633–641.
4. Alsop DC, Detre JA, Grossman M. Assessment of cerebral blood flow in Alzheimer's disease by spin-labeled magnetic resonance imaging. Ann Neurol 2000;47:93–100.
5. Edelman RR, Siewert B, Darby DG, Thangaraj V, Nobre AC, Mesulam MM, Warach S. Qualitative mapping of cerebral blood flow and functional localization with echo-planar MR imaging and signal targeting with alternating radio frequency. Radiology 1994;192:513–520.
6. Edelman RR, Chen Q. EPISTAR MRI: multislice mapping of cerebral blood flow. Magn Reson Med 1998;40:800–805.
7. Kwong KK, Chesler DA, Weisskoff RM, Donahue KM, Davis TL, Ostergaard L, Campbell TA, Rosen BR. MR perfusion studies with T1-weighted echo planar imaging. Magn Reson Med 1995;34:878–887.
8. Kim SG. Quantification of relative cerebral blood flow change by flow-sensitive alternating inversion recovery (FAIR) technique: application to functional mapping. Magn Reson Med 1995;34:293–301.
9. Wong EC, Buxton RB, Frank LR. Implementation of quantitative perfusion imaging techniques for functional brain mapping using pulsed arterial spin labeling. NMR Biomed 1997;10:237–249.
10. Pekar J, Jezzard P, Roberts DA, Leigh Jr JS, Frank JA, McLaughlin AC. Perfusion imaging with compensation for asymmetric magnetization transfer effects. Magn Reson Med 1996;35:70–79.
11. Jezzard P, Balaban RS. Correction for geometric distortion in echo planar images from B0 field variations. Magn Reson Med 1995;34:65–73.
12. Luh WM, Wong EC, Bandettini PA, Hyde JS. QUIPSS II with thin-slice TI1 periodic saturation: a method for improving accuracy of quantitative perfusion imaging using pulsed arterial spin labeling. Magn Reson Med 1999;41:1246–1254.
13. Wong EC, Buxton RB, Frank LR. A theoretical and experimental comparison of continuous and pulsed arterial spin labeling techniques for quantitative perfusion imaging. Magn Reson Med 1998;40:348–355.
14. Tanabe JL, Youngbi M, Branch C, Hrabe J, Johnson G, Helpern JA. MR perfusion imaging in human brain using the UNFAIR technique. J Magn Reson Imaging 1999;9:761–767.
15. Lai S, Wang J, Jahng GH. FAIR exempting separate T_1 measurement (FAIREST): a novel technique for online quantitative perfusion imaging and multi-contrast fMRI. NMR Biomed 2001;14:507–516.
16. Haralick RM, Shanmugam K, Dinstein I. Textural features for image classification. IEEE Trans Syst Man Cybernet 1973;3:610–621.
17. Duyn JH, Tan CX, van Gelderen P, Yongbi MN. High-sensitivity single-shot perfusion-weighted fMRI. Magn Reson Med 2001;46:88–94.
18. Matson GB. An integrated program for amplitude-modulated RF pulse generation and re-mapping with shaped gradients. Magn Reson Imaging 1994;12:1205–1225.
19. Bucciolini M, Ciraolo L, Renzi R. Relaxation rates of paramagnetic solutions: evaluation by nuclear magnetic resonance imaging. Med Phys 1986;13:298–303.

20. Ross JS, Masaryk TJ, Modic MT. Three-dimensional FLASH imaging: applications with gadolinium-DTPA. J Comput Assist Tomogr 1989;13: 547–552.
21. Prendergast DJ. Analysis of magnetic resonance images. MS thesis, University of Manchester, 1986.
22. Raeth U, Schlaps D, Limberg B, Zuna I, Lorenz A, Dipl-Ing, van Kaick G, Lorenz WJ, Kommerell B. Diagnostic accuracy of computerized B-scan texture analysis and conventional ultrasonography in diffuse parenchymal and malignant liver disease. J Clin Ultrasound 1985;13: 87–99.
23. Golay X, Stuber M, Pruessmann KP, Meier D, Boesiger P. Transfer insensitive labeling techniques (TILT): application to multislice functional perfusion imaging. J Magn Reson Imaging 1999;9:454–461.
24. Matson GB, Schleich T. Design of null pulses for use in pulsed arterial spin labeling by the principle of time reversal. In: Proceedings of the 9th Annual Meeting of ISMRM, Glasgow, Scotland, 2001. p 687.
25. Frank LR, Wong EC, Buxton RB. Slice profile effects in adiabatic inversion: application to multislice perfusion imaging. Magn Reson Med 1997;38:558–564.
26. Keilholz-George SD, Knight-Scott J, Berr SS. Theoretical analysis of the effect of imperfect slice profiles on tagging schemes for pulsed arterial spin labeling MRI. Magn Reson Med 2001;46:141–148.
27. Lei H, Peeling J. A strategy to optimize the signal-to-noise ratio in one-coil arterial tagging perfusion imaging. Magn Reson Med 1999;41: 563–568.
28. Yang Y, Frank JA, Hou L, Ye FQ, McLaughlin AC, Duyn JH. Multislice imaging of quantitative cerebral perfusion with pulsed arterial spin labeling. Magn Reson Med 1998;39:825–832.
29. Ye FQ, Frank JA, Weinberger DR, McLaughlin AC. Noise reduction in 3D perfusion imaging by attenuating the static signal in arterial spin tagging (ASSIST). Magn Reson Med 2000;44:92–100.
30. Jagust WJ, Ebering JL, Reed BR, Mathis CA, Budinger TF. Clinical studies of cerebral blood flow in Alzheimer's disease. Ann NY Acad Sci 1997;826;254–262.